Journal of Controlled Release 172 (2013) 993–1001

Contents lists available at ScienceDirect

Journal of Controlled Release

journal homepage: www.elsevier.com/locate/jconrel

NANOMEDICINE

Rubik-like magnetic nanoassemblies as an efficient drug multifunctional carrier for cancer theranostics

Fei Xiong [a], Yuejian Chen [a], Jianxiang Chen [b], Bingya Yang [b], Yu Zhang [a], Huile Gao [c], Zichun Hua [b], Ning Gu [a,*]

[a] State Key Laboratory of Bioelectronics, Jiangsu Laboratory for Biomaterials and Devices, School of Biological Science and Medical Engineering, Southeast University, Nanjing, China
[b] State Key Laboratory of Pharmaceutical Biotechnology, Nanjing University, Nanjing, China
[c] Key Laboratory of Smart Drug Delivery, Ministry of Education & PLA, Department of Pharmaceutical Sciences, School of Pharmacy, Fudan University, Shanghai, China

ARTICLE INFO

Article history:
Received 30 May 2013
Accepted 24 September 2013
Available online 2 October 2013

Keywords:
Iron oxide nanocubes
Magnetic nanoassemblies
Paclitaxel
Magnetic resonance image
Cancer therapy

ABSTRACT

A practical and effective strategy for loading hydrophobic anticancer agents within the inside and outside oleic acid layer of Rubik-like magnetic nanoassemblies (MNAs) is established. In this strategy, four individual oleic acid-capped iron oxide nanocubes and dioleate-modified polyethylene glycol are assembled into cluster with high drug loading capability, high magnetism, as well as rapid and extended release behavior. After loading model drug paclitaxel (PTX), PTX-MNAs show greater antitumor activity both *in vitro* cell culture and *in vivo* animal trials compared with the same dose of free PTX (Taxol). With high uptake by tumor cells, MNAs exhibit in tumor imaging by magnetic resonance imaging. These outstanding properties are largely due to the drug delivery systems that take high drug-loading capability and high magnetism into consideration in a nano-dimension for maximizing the nanotheranostic functions and minimizing the toxic side effects. In summary, the Rubik-like magnetic nanoassemblies may have the potential to realize "all-in-one" nanotheranostic strategy to detect, diagnose, treat, and monitor tumors and therapeutic response in further pre-clinical and clinical studies.

1. Introduction

Short comings of currently conventional systemic chemotherapy include limited therapeutic efficacy, inability to produce and maintain a therapeutic concentration of drug into a localized pathological site, toxicity to non-targeted tissues and no means of simultaneous visible detection or imaging. The emergence of multifunctional magnetic nanoparticles these years attracted a great deal of attention and anticipation into the realm of cancer nano-theranostic modalities. Of the different types of magnetic nanoparticles, typically single spheres, surface engineered superparamagnetic iron oxide nanoparticles (SPIONs) have enabled better localized targeting of drugs, a means of visualization through magnetic resonance imaging (MRI) and an apoptotic effect on cancer cells through localized hyperthermia as a result of the magnetic properties in conjunction with the drug delivery component of the nanoparticles [1–4]. Desirably, a high magnetic response is therefore essential in magnetism based multiple biomedical functions and is directly proportional to the size of the nanoparticle. However, although numerous chemical means of drug loading have been achieved, the ability to produce a large, rapid and controlled release of drug within therapeutic range is problematic in that higher drug loading capacity is related to particle surface area. Smaller particles provide more surface area and are therefore more suitable for drug loading but at the expense of magnetic properties. The challenge therefore was to construct a drug delivery system that combined a high drug loading capacity with greater magnetic properties in a nano-dimension for maximizing the theranostic properties of the system.

We propose a nano-carrier platform for delivering hydrophobic anticancer drugs to tumors through the formation of Rubik-like magnetic nanoassemblies (MNAs) utilizing a solvent-exchanging assembly procedure (Fig. 1). The nanoassemblies are multiple core/shell structures composed of hydrophobic oleic acid-capped magnetic Fe_3O_4 nanocubes (Fe_3O_4@OA NCs, core) and amphiphilic dioleate-modified polyethylene glycol (OA_2-PEG, shell). Compared to spherical particles, cubes provide a greater surface area to volume ratio providing enhanced loading of small hydrophobic molecules in the OA layer for concentrated drug delivery. Magnetic dipole–dipole interactions of assembled nanoparticulate structures are much stronger than those of individual nanoparticles [4], therefore the aggregated SPIONs can provide even higher contrast than individually dispersed SPIONs as MRI contrast agent [5–10]. In some published literatures [5,6,11], the T_2 relaxivity (r_2) value of clustered nanoparticles can be more than 18-times higher than that of individual nanoparticles under the same iron concentration. Assembly of several smaller nanocubes into one cluster produces a greater magnetic response than the summation of each individual nanocubes. Cube clusters also provide for added surface area and greater drug loading as compared to a single larger cube. Although drug release from the outer exposed OA-layer of MNAs is rapid and constitutes a burst effect, the inner surfaces of adjacent cubes provide protection from the burst effect

* Corresponding author. Tel.: +86 25 83272476; fax: +86 25 83272460.
E-mail address: guning@seu.edu.cn (N. Gu).

0168-3659/$ – see front matter © 2013 Elsevier B.V. All rights reserved.
http://dx.doi.org/10.1016/j.jconrel.2013.09.023

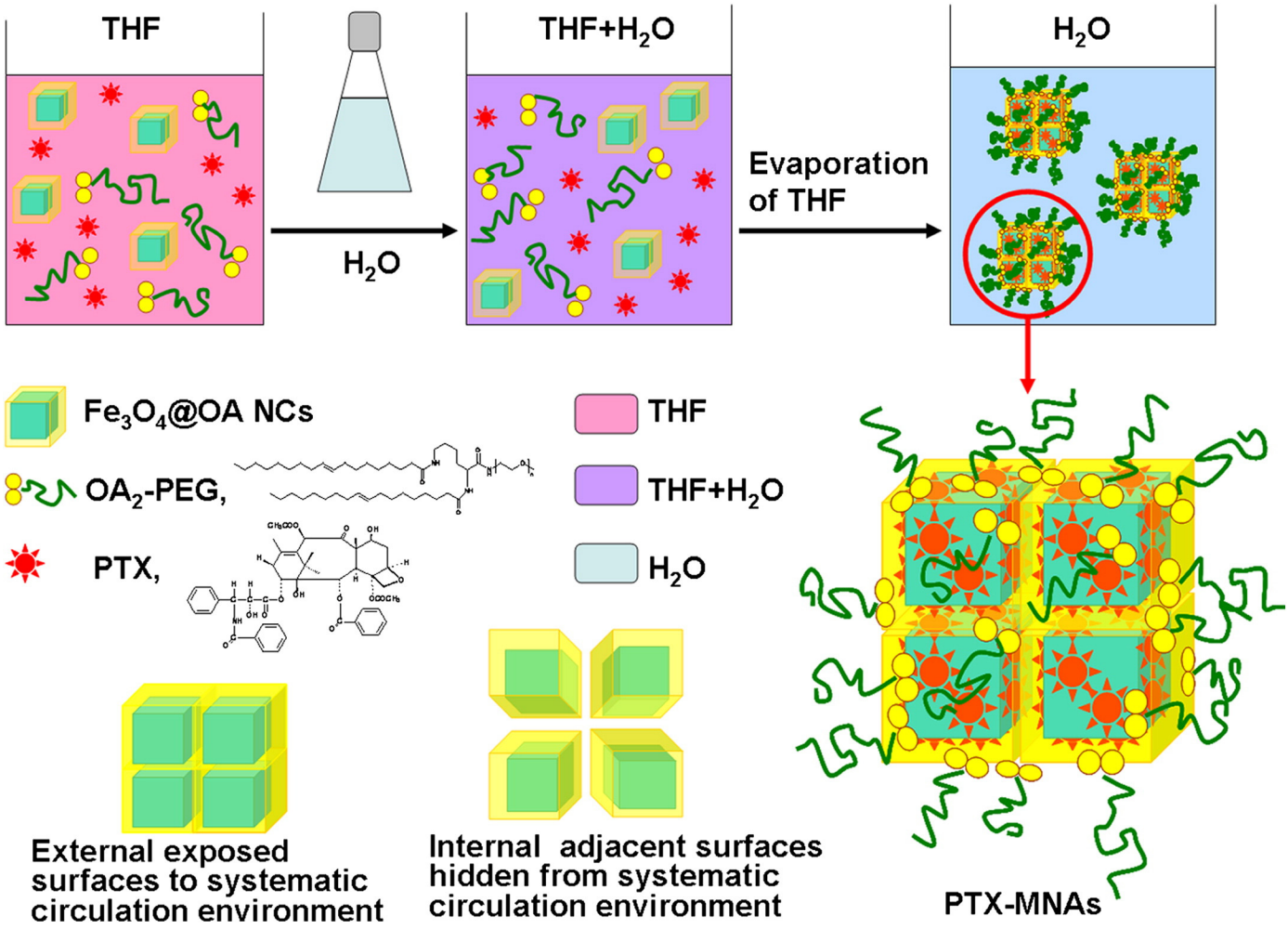

Fig. 1. Schematic representing formulation and structure of Rubik like PTX-MNAs. Upon encapsulation in nanoassemblies, the hydrophobic PTX was inserted in the oleic acid cap of Fe_3O_4@OA NCs. The polymers were anchored on the surface of Rubik cube like nanoassemblies by the hydrophobic interaction between oleic acid cap of Fe_3O_4 NCs and oleic acid terminal of amphiphilic polymers.

and enable a higher concentration of drug to be released at a later time when the cubes have reached their targeted location. Hence rapid and sustained therapy can both be achieved in one nano-drug delivery system. To realize the effective delivery, the nanoassemblies must also possess other properties such as optimal hydrodynamic particle size, high hydrophilic surface for EPR (enhanced permeability and retention)-effect, remain in circulation sufficiently to reach the intended target and to escape being rapidly opsonized and massively cleared by the reticuloendothelial system (RES) of the liver and spleen as well as macrophages of mononuclear phagocyte system (MPS) tissues such as the lungs and the bone marrow.

In this paper, we used paclitaxel as model drug and constructed drug-loaded MNAs (PTX-MNAs). Compared with a commonly used commercial preparation of paclitaxel (Taxol), the results presented here show that multifunctional capacities within a single nano-assembled material have a number of potential applications in targeted drug delivery and MRI for tumor diagnosis and therapy in clinic.

2. Materials and methods

2.1. Materials and animals

Paclitaxel was purchased from Jiangsu Yew Pharmaceutical Co., Ltd. (Wuxi, China, purity > 99%). Taxol injection purchased from Yangtze River Pharmaceutical Group Jiangsu Pharmaceutical Trading Co., Ltd. (Jiangsu, China). Fluorescein (2-(6-hydroxy-3-oxo-3h-xanthen-9-yl)-benzoic acid, $C_{20}H_{12}O_5$) was purchased from Aladdin Chemical Reagent Company (Wuhan, China). RAW264.7 and B16F10 cells were purchased from Shanghai Cellular Institute of China Scientific Academy (Shanghai, China). Apoptosis PI Detection Kit was purchased from KeyGen Biotech Co. Ltd. (Nanjing, China). Meso-2, 3-dimercaptosuccinic acid-coated γ-Fe_3O_4 nanoparticles were provided by our lab. 3-(4,5-Dimethyl thiazol-2-yl)-2,5-diphenyl tetrazolium bromide (MTT) was purchased from Fluka (MO, USA).

C57BL/6 mice were purchased from Shanghai Laboratory Animal Center of the Chinese Academy of Sciences and maintained at 22 ± 2 °C on a 12 h light–dark cycle with access to food and water *ad libitum*. The animals used for the experiment were treated according to the protocols evaluated and approved by the ethical committee of Nanjing University (Nanjing, China).

2.2. Preparation of PTX-MNAs

Fe_3O_4@OA NCs were synthesized through the decomposition of iron-oleate complexes at 300 °C using octadecene as the solvent by previously developed methods [12]. OA_2-PEG with PEG number average molecular weight of 2000 was synthesized through lysine linkage and esterification following the published procedure [13]. For preparation

of PTX-MNAs, PTX, Fe_3O_4@OA NCs and OA_2-PEG were dissolved in tetrahydrofuran (THF) at a weight ratio of 1:5:55 under sonication. The mixture was slowly added into double distilled water under sonication in an ice water bath and the resulting suspension was stirred for 6 h to evaporate THF. Then the suspension was dialyzed against water to remove the remaining drug. The loading of drug in PTX-MNAs was 12 wt.% (PTX/Fe).

2.3. Characterization

The morphological structure of PTX-MNAs dispersed in double distilled water was analyzed using TEM with negative staining by 2% phosphotungstic acid. The hydrodynamic diameter, size distribution and zeta potential of PTX-MNAs were examined using TEM and Zeta PALS instrument (Brookhaven Instrument Corporation) by dynamic light scattering (DLS) and electrophoretic mobility at 25 °C. To determine the kinetics of PTX release from particles, 1 mL of PTX-MNAs was added to 1 mL fresh rat plasma and the mixture was placed in dialysis bag (8000–10000 molecular weight cutoff). The dialysis bag was immersed in 100 mL of pH 7.4 phosphate buffer or pH 4.5 acetate buffer (both of release medium containing 0.5% v/v Tween 80) shaked continuously at 37 °C. One milliliter aliquots of release medium were removed and the same volume of fresh medium was added periodically. Twenty-microliter aliquots of the released drug were quantified at 227 nm by HPLC using a reverse-phase C18 column (250 mm × 4.6 mm, 5 μm particle size; Hanbon Sci. & Tech., Huaian, China), with methanol–water (75:25, v/v) as mobile phase at 40 °C at a flow-rate of 1.0 mL/min. Magnetic properties were measured with a vibrating sample magnetometer (VSM, Lakeshore 7407, USA) in a field up to 5 kOe.

2.4. Determination of drug in biosamples

Quantification of drug in cells, plasma, tumors and tissues was performed as follows. Cells were sonicated in 1 mL of acetonitrile and centrifugated at 16,000 rpm at 4 °C for 10 min. The supernatant obtained was analyzed for drug uptake in cells using HPLC. A 100 μL aliquot of homogenate (20%, w/v) of tumors or tissues in physiological saline was performed with a potter on ice. A 300 μL aliquot of acetonitrile was added into 100 μL of homogenate or plasma to precipitate protein. Then, the samples were mixed with shaking on a vortex shaker for 5 min. After centrifugation for 10 min and 16,000 ×*g* at 4 °C, a 20 μL aliquot of the supernatant fluid was injected into HPLC for assay. The chromatographic system consisted of a Shimadzu LC-20AT system (Shimadzu Corp., Kyoto, Japan), incorporating 20 AD pump and SPD-20A diode array detector. The wavelength of this detector was set to 227 nm. The HPLC system was controlled by a computer employing the Millennium 2010 ChemStation software. The analytical column was a reverse phase Hypersil C_{18} column (250 × 4.6 mm, 5 μm particle size; Shimadzu Corp., Kyoto, Japan) maintained in a 20A column oven and protected by a guard column (10 × 4.6 mm, Shimadzu Corp., Kyoto, Japan) packed with the same material. The mobile phase was composed of methanol–water (72:28, v/v). Elution was performed isocratically at 40 °C at a flow-rate of 1.0 mL/min.

2.5. In vitro performance of PTX-MNAs

2.5.1. Uptake of vehicles by macrophage cells

RAW 264.7 cells were seeded in 24-well plates at density of 1×10^5 cells per well and left overnight. After exposure to MNAs at concentrations of 50, 100, and 200 μg Fe/mL in medium at 37 °C for 1 h, some cells were washed, dissolved and analyzed for iron levels using 1,10-phenanthroline colorimetric method. Other cells were fixed with 2.5% glutaraldehyde and stained by Prussian blue (4% potassium ferric-ferrocyanide in 4% HCl) and nuclear fast red, which indicates the presence of iron and cell nuclear. Then cells were washed and visualized for vehicle internalization using light microscopy (Axioplan Imaging II, Zeiss, Göttingen, Germany). The cells without being incubated with MNAs were observed as control.

2.5.2. Penetration and cytotoxicity of PTX-MNAs in melanoma cells

B16F10 cells were seeded in 6-well plates and allowed to adhere overnight. The medium was then replaced with 2 mL medium containing 1.0, 2.0 and 4.0 μg PTX/mL of Taxol (Yangtze River Pharmaceutical Group Jiangsu Pharmaceutical Trading Co., Ltd., China), PTX-MNAs in the absence and presence of neodymium–iron–boron (NdFeB) permanent magnet (remanence Br = 0.52 T) placed beneath the cell plates incubated for 4 h. After centrifugation of detached cells, the precipitation was disposed and analyzed for drug concentration using HPLC as mentioned below and for iron levels using 1,10-phenanthroline colorimetric method. Cell viability was evaluated according to mitochondrial conversion by using a 3-[4,5-dimethylthiazol-2-yl]-2,5-diphenyl tetrazolium bromide (MTT).

To assay the penetration and MRI efficiency of vehicles *in vitro*, B16 F10 cells incubated for 4 h with 4 μg/mL of PTX-MNAs in the absence and presence of a magnet were washed, trypsinized and resuspended in 2% agarose solution for imaging on a clinical 1.5 Tesla MRI scanner (Magnetom Avanto, Siemens, Germany) with a 12-channel head coil at room temperature. Water and cells incubated with Taxol were also tested as control. The sequence included a fast spin-echo sequence: repetition time (TR) = 5500 ms, echo time (TE) = 100 ms; field of view (FOV) = 50 mm × 50 mm; slice thickness = 2 mm.

2.6. In vivo theranostic effects

2.6.1. In vivo antitumor efficacy of PTX-MNAs

C57BL/6 mice (6–8 weeks of age) were implanted subcutaneously in the left flank with B16F10 cells (10^6 cells/mouse) in 0.2 mL PBS. When the mean volume of melanoma tumor reached 200–300 mm^3, the mice were divided into four groups and administered by a single tail vein injection of one of the following samples: saline (0.9% sodium chloride), Taxol injection (10 mg PTX/kg), and PTX-MNAs (10 mg PTX/kg) in the absence of a NdFeB permanent magnets and in the presence of a magnet placed over the tumor for 0.5 h (PTX-MNAs-M) after injection under anesthesia. Five mice were killed by cervical vertebra dislocation at one day after injection, and their tumors were harvested and measured with vernier calipers. Another five mice were used for daily monitoring tumor measured individually. At day 8 after injection, these five mice were killed and their tumors were processed and analyzed. The remaining five tumor-bearing mice in each group were checked for survival analysis every day. The tumor volumes were calculated using the formula: (the largest diameter) × (the smallest diameter)^2 × 0.5. Therapeutic effects on tumor growth were expressed as the ration of mean tumor volume in treated mice (T) divided by that of control group (C) *versus* time and tumor inhibition rate (TIR), which was calculated by the following formula: TIR (%) = (tumor volume of saline group − tumor volume of drug group)/tumor volume of saline group. Apoptosis was determined with the terminal deoxynucleotidyl transferase-mediated deoxyuridine triphosphate nick-end labeling (TUNEL) assay for the identification of double-stranded DNA breaks with an *in situ* cell death detection kit according to the manufacturer's instructions.

2.6.2. In vivo MRI in tumor-bearing mice

At 2 h after injection, mice were anesthetized and placed in the center of a clinical 1.5 Tesla MRI scanner (Magnetom Avanto, Siemens, Germany). The sequence was the same as that mentioned above except for FOV = 14 cm × 14 cm. The signal intensities of PTX-MNAs-incubated cells or -injected mice in the absence and presence of magnets were determined from a circular 10-mm^2 region of interest (ROI).

2.7. Pharmacokinetics and biodistribution of PTX-MNAs in tumor-bearing mice

At 0.25, 0.5, 1, 2, 4, 8, 12 and 24 h after injection, the three animals of each group were sacrificed under ether anesthesia. Blood was collected in heparin-coated tubes and centrifuged at 1500 rpm for 5 min. Tumor, liver and kidneys were removed, weighed and homogenized in physiological saline. To further evaluate efficiency of tumor targeting, the areas under the plasma and tissue concentration–time curves (AUC) of PTX-MNAs or PTX-MNAs-M were divided by the AUC of Taxol in certain tissue. Re relative exposure (Re) was expressed as follows: $Re_{PTX\text{-}MNAs} = AUC_{PTX\text{-}MNAs} / AUC_{Taxol}$, $Re_{PTX\text{-}MNAs\text{-}M} = AUC_{PTX\text{-}MNAs\text{-}M} / AUC_{Taxol}$. The vehicle distribution in tumors and tissues was also visualized by Prussian blue staining. The subcellular localization of vehicles in tumors was examined with TEM.

2.8. Safety assay

To study the toxic effects of PTX-MNAs treatment, 24 healthy mice (body weight = 18–22 g) were randomly divided into 4 groups (6 mice per group, free access to food and water) and administered three doses on days 0, 4, and 8 through tail vein injection of one of the following samples: saline, Taxol injection (10 mg PTX/kg), and PTX-MNAs (10 mg PTX/kg) in the absence and presence of a magnet placed on the left side of flank for 0.5 h after injection under anesthesia. The body weight was recorded daily and tissue sections were prepared for histopathological analysis. In details, on day 12 (4 days after last administration), the liver and kidneys were harvested and processed routinely into paraffin, sectioned at a thickness of 5 μm, and stained with haematoxylin and eosin (HE) staining.

3. Results and discussion

3.1. Preparation and characterization of PTX-MNAs

Although encapsulating antitumor drug into magnetic nanoparticles has shown promise as a means of achieving multifunctional theranostics of tumors in animal models, the possibilities of combination of high drug-loading capability and high magnetism together into one nano-sized depot had not been explored. This is the first report about the use of Rubik cube-like magnetic assemblies as a drug delivery system. The strategy of developing PTX-loaded MNAs using a solvent-exchanging assembly procedure was shown schematically in Fig. 1. Although the drug is not chemically conjugated to Fe_3O_4@OA NCs, strong hydrophobic interactions with the OA layer of the Fe_3O_4@OA NCs trap the drug within the nanoparticles, preventing its rapid leaching, making the MNAs a promising candidate for tumor long-lasting therapy. Monodispersed Fe_3O_4@OA NCs provide fixed dimension for drug loading and thus decrease the difference of drug-loading efficiency between batches.

Physical properties of the PTX-MNAs following the solvent-exchanging assembly procedure were revealed by transmission electron microscopy (TEM). The TEM of Fe_3O_4@OA NCs dispersed in n-hexane was shown in Fig. 2A. Four individual Fe_3O_4@OA NCs with 10.2 ± 0.7 nm diameter were assembled into PTX-MNAs, and the average size of assemblies and its shell were 40–50 nm and 2–3 nm, respectively (Fig. 2B). The hydrodynamic diameter of PTX-MNAs measured by dynamic light scattering (DLS) was 61.9 ± 2.0 nm (Fig. 2C), which was the total diameter of an assembly and its aqueous layer thickness. The hydrodynamic diameter is small enough to penetrate into the tumor tissues according to the reported size range of 20–200 nm in which nanocarriers could extravasate and accumulate maximally to distal tumor sites following intravenous injection *via* the EPR effect [11].

The drug release rate from nanoassemblies in the presence of fresh rat plasma was affected by release time and the pH value of release medium (Fig. 2D). The external exposed surfaces of PTX-MNAs to systematic circulation environment resulted in faster drug release, while the internal adjacent surface hidden from systematic circulation environment resulted in slower drug release. Consistently, about 43% of total drug was released in the former 48 h of incubation, while about only 16% drug of total drug was release in the latter 48 h, thus indicating rapid-released and sustained released drugs were both realized in this system. After 96 h of incubation, 65.73 ± 2.82% of total drug was released in the medium at pH 4.5 compared with the 52.57 ± 3.18% released in the medium at pH 7.4, suggesting that after internalization into tumor cells, the acidic environment in endolysosome might benefit the release of PTX from nanoassemblies. PTX generally behaves as a weak organic alkaline and is more soluble in an acid than in an alkaline environment, therefore PTX-MNAs released the drug in a pH-dependent manner.

In addition, assembly of several magnetic nanocubes into one cluster is effective to prepare MRI probe with high relaxivity for tumor detection. The hysteresis loop of assembled PTX-MNAs is shown in Fig. 2E and the saturation magnetization (Ms) value of assembled PTX-MNAs is 69.90 emu/g. Magnetic measurements indicated superparamagnetic behavior of PTX-MNAs at room temperature, as evidenced by zero coercivity and remanence on the magnetization loops and the Ms of PTX-MNAs was enough to be used as MRI probe. The high magnetic response of cluster is also a guarantee for enhanced magnet-mediated intracellular drug uptake with applying an external magnetic field, and the assembled Fe_3O_4@OA NCs are thus better suited for magnetic-induced targeting in the next research.

3.2. In vitro performance of PTX-MNAs

3.2.1. Effects of surface molecular phagocytosis by RAW 264.7 macrophage cells

Raw 264.7 cells are a kind of macrophage cells. Fe_3O_4 NPs can be made to evade RES, MPS and attain a long blood circulation time to reach other target organs by PEG coating. To assess the ability of OA_2-PEG-coated MNAs to escape macrophage (RES and MPS) uptake, *in vitro* phagocytosis experiments were conducted using RAW 264.7 cells prior to *in vivo* studies. To assess the impact of surface coating on uptake, cells were also exposed to small molecular meso-2, 3-dimercaptosuccinic acid-coated Fe_3O_4 nanoparticles (Fe_3O_4@DMSA NPs) with similar diameter [14]. Most of the RAW 264.7 cells incubated with 100 μg/mL of Fe_3O_4@DMSA NPs for 1 h exhibited blue staining, while few blue spots were detected in the cytoplasm of the cells incubated with polymer coated-MNAs under the same conditions (Fig. 3A). Based on this approach, OA_2-PEG coating can effectively prevent the uptake of iron oxide nanoparticles by macrophages, and can achieve long circulation in blood stream and shield for nanoparticles from being rapidly opsonized and massively cleared by RES and MPS (liver, spleen, lungs and bone marrow) rich organs before reaching tumor.

3.2.2. In vitro cellular penetration and cytotoxicity of PTX-MNAs

PTX is a mitotic inhibitor used in cancer chemotherapy, including ovarian cancer, breast cancer, melanoma and so on in clinic. B16F10 cells are a kind of malignant melanoma cells. Therefore, we used B16F10 melanoma cells as a model cell to study the extent of drug penetration and cytotoxicity *in vitro* after loading PTX into MNAs and investigate whether PTX-MNAs were effective against an established melanoma *in vivo*. The extent of drug penetration and cytotoxicity was demonstrated on B16F10 melanoma cells by loading PTX into MNAs. The cellular PTX content increased strongly after exposure of the cells to PTX-MNAs from 0.49 ± 0.13 to 1.30 ± 0.17 pg/cell compared with cells exposed to the same concentration of Taxol (0.28 ± 0.07 to 0.80 ± 0.15 pg/cell)(Fig. 3B). To study the effects of an external magnetic field on the intracellular accumulation of PTX-MNAs, the cells were incubated with the same concentration of PTX-MNAs in the presence of a magnet (PTX-MNAs-M) underneath the cells. The cellular PTX values were significantly (0.53 ± 0.14 to 1.48 ± 0.26 pg/cell)

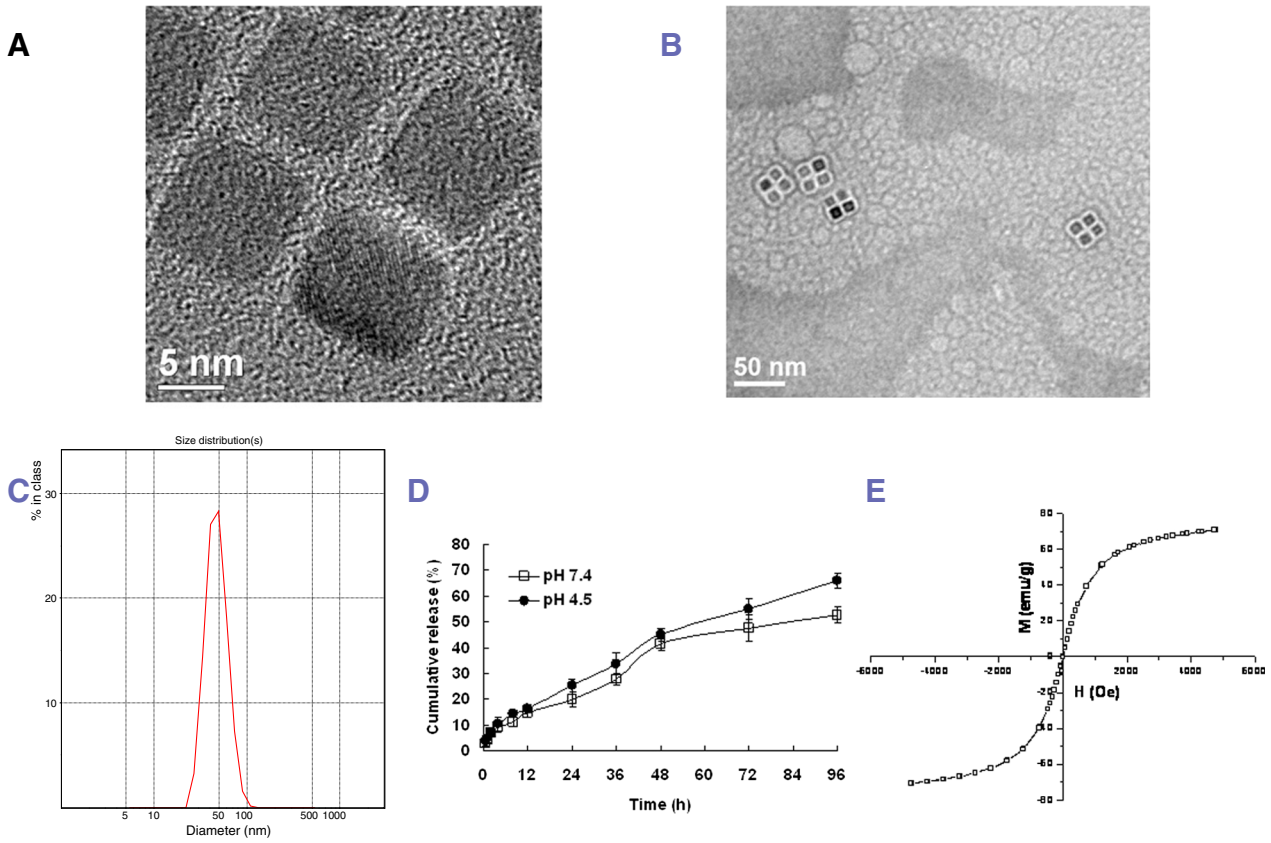

Fig. 2. Characterization of PTX-MNAs. A) The TEM of Fe_3O_4@OA NCs dispersed in n-hexane. B) Typical TEM image of Rubik like PTX-MNAs dispersed in double distilled water. C) Hydrodynamic diameter distribution of PTX-MNAs in double distilled water. D) Time course of PTX release from MNAs at 37 °C at pH 4.5 (open squares) or 7.4 (filled circles). Released PTX was separated from PTX-MNAs by dialysis and quantified using HPLC. Each point represents average ± SD ($n = 3$). E) Hysteresis loops of PTX-MNAs measured at room temperature.

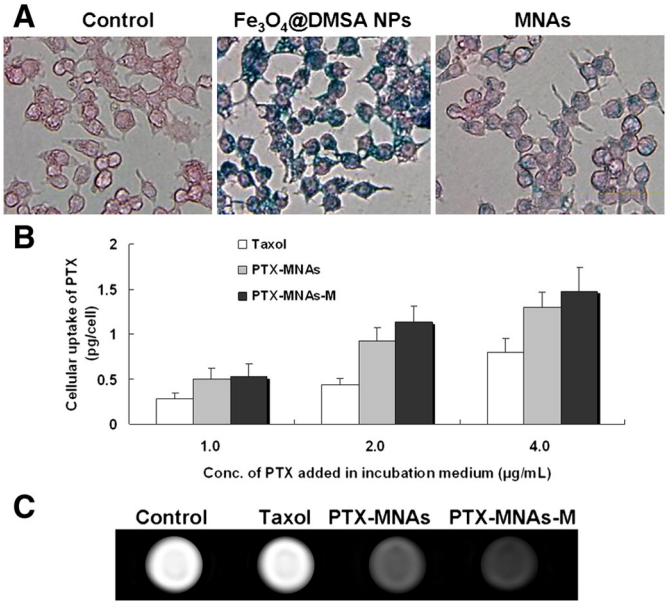

Fig. 3. *In vitro* cellular uptake and toxicity studies. A) Cellular uptake of Fe_3O_4@DMSA NPs and MNAs in RAW 264.7 cells. Prussian blue and nuclear fast red double staining images of cells at concentrations of 100 μg Fe/mL in medium at 37 °C for 1 h (magnification 400×). Penetration of the PTX-MNAs in B16F10 melanoma cells. B) Quantification of internal PTX in B16F10 cells after 4 h of exposure to 1.0, 2.0 and 4.0 μg/mL of Taxol (free paclitaxel, white columns), PTX-MNAs in the absence (light gray columns) and presence (dark gray columns) of a magnet at 37 °C. Each point represents average ± SD. ($n = 3$). C) T_2-weighted magnetic resonance images of B16F10 cells cultured with Taxol, PTX-MNAs in the absence and presence of a magnet and resuspended in 2% agarose solution. The agarose solution was also used as control.

higher than those obtained by incubations without a magnet. These experiments demonstrate that MNAs could facilitate intracellular delivery of PTX into B16F10 cancer cells and the magnetic feature can be exploited to optimize the cellular uptake. The IC_{50} values determined by MTT method were 86.3 ± 5.2 ng/mL, 54.8 ± 4.6 ng/mL, and 39.6 ± 5.7 ng/mL for Taxol, PTX-MNAs and PTX-MNAs-M, respectively. It was worth noting that the corresponding excipient concentration of PTX-MNAs was almost not toxic to the B16F10 cells, while the corresponding Cremophor/ethanol carrier mixture of Taxol significantly affected the viability of cells (data not shown). These results suggest that it does not only maintain the cancer cell destruction ability of PTX, but also efficient delivery of drug to the cells and more effective in the presence of a magnet.

Using a clinical 1.5-T MRI scanner, the mean T_2 relaxation time of B16F10 cells in agarose incubated with PTX-MNAs and PTX-MNAs-M (Fig. 3C) was significantly decreased (425.2 ± 21.5 and 336.4 ± 19.3 ms, respectively) compared with water and cells incubated with Taxol (no MR contrast). The results indicated the potential of MNAs to serve as a sensitive MRI contrast agent.

3.3. *In vivo* theranostic effects

3.3.1. *Antitumor effect of PTX-MNAs in the B16 F10 melanoma-bearing C57BL/6 mice*

To investigate whether PTX-MNAs were effective against an established melanoma *in vivo*, B16F10 cells were injected subcutaneously into C57BL/6 mice. On day 0, the mice were injected intravenously in single dose with saline (0.9% sodium chloride), Taxol (10 mg PTX/kg), PTX-MNAs (10 mg PTX/kg) and PTX-MNAs-M (a magnet placed over the tumor for 0.5 h after injection under anesthesia, 10 mg PTX/kg). On day 8, the tumors in mice treated with PTX-MNAs-M were much smaller

than in comparison with the other three groups (Fig. 4A), and the tumor inhibition rates (TIR%) of Taxol, PTX-MNAs and PTX-MNAs-M group were 58.67%, 70.73% and 78.74%, respectively. In a Kaplan–Meier curves (Fig. 4B), the mean survival time of PTX-MNAs-M group was 21.6 days compared with 19 days for PTX-MNAs group, 15.6 days for Taxol group, and 13.6 days in the saline control group. To evaluate apoptotic effects within the tumor cell isolated from mice melanoma models, TUNEL assay was used to detect DNA fragmentation. The results shown in Fig. 4C (arrows) illustrate increased apoptotic events following treatment with PTX-MNAs, especially in the presence of an external magnetic field. These results indicate that PTX-MNAs repressed tumor growth and prolonged the mice survival to a greater extent than Taxol, and PTX-MNAs-M exhibited the strongest antitumor activity and the longest mean survival time.

Based on these, the increased cellular toxicity, increased apoptosis events and decreased tumor size could be further explained by the intracellular localization to acidic environment within lysosomes where more drug is released from MNAs than that in neutral environment of blood and other tissues.

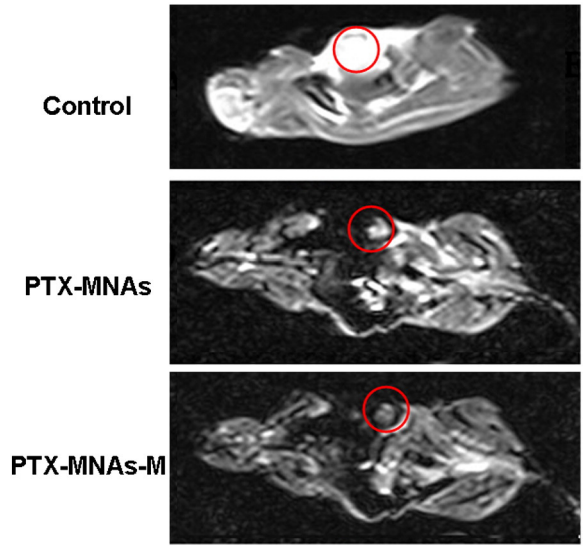

Fig. 5. T_2-weighted magnetic resonance images of B16F10 cells-bearing C57BL/6 mice treated with saline, PTX-MNAs in the absence and presence of a magnet (PTX-MNAs-M).

3.3.2. In vivo MRI

To assess the application potentials of PTX-MNAs in tumor imaging and accumulation ability of vehicles in tumor-bearing mice, the MRI of mice treated with PTX-MNAs and PTX-MNAs-M was conducted at 2 h post-injection with dose of 10 mg PTX/kg *via* tail vein. For Taxol-treated control group, no significant decrease of MRI signal intensity in tumor area is observed (Fig. 5, control, arrow, T_2 value = 441.4 ± 13.7 ms), whereas the signal intensity in the tumor of mice treated with PTX-MNAs and PTX-MNAs-M dropped dramatically (T_2 value = 304.4 ± 42.7 and 223.1 ± 33.7 ms, respectively). These results indicate that the MNAs-based drug carriers produce a significant difference of imaging contrast after extravasating through leaky neo-vasculature of tumor tissue. The contrast-enhanced imaging can potentially enhance the efficacy of early diagnosis and timely therapeutic intervention.

3.4. Pharmacokinetics and biodistribution of PTX-MNAs

To investigate the basis of the increased effectiveness in tumor growth suppression and reduced toxicity, we determined the pharmacokinetics and distribution of PTX in the systemic circulation, tumor and other tissues. The C57BL/6 mice bearing B16F10 tumors were

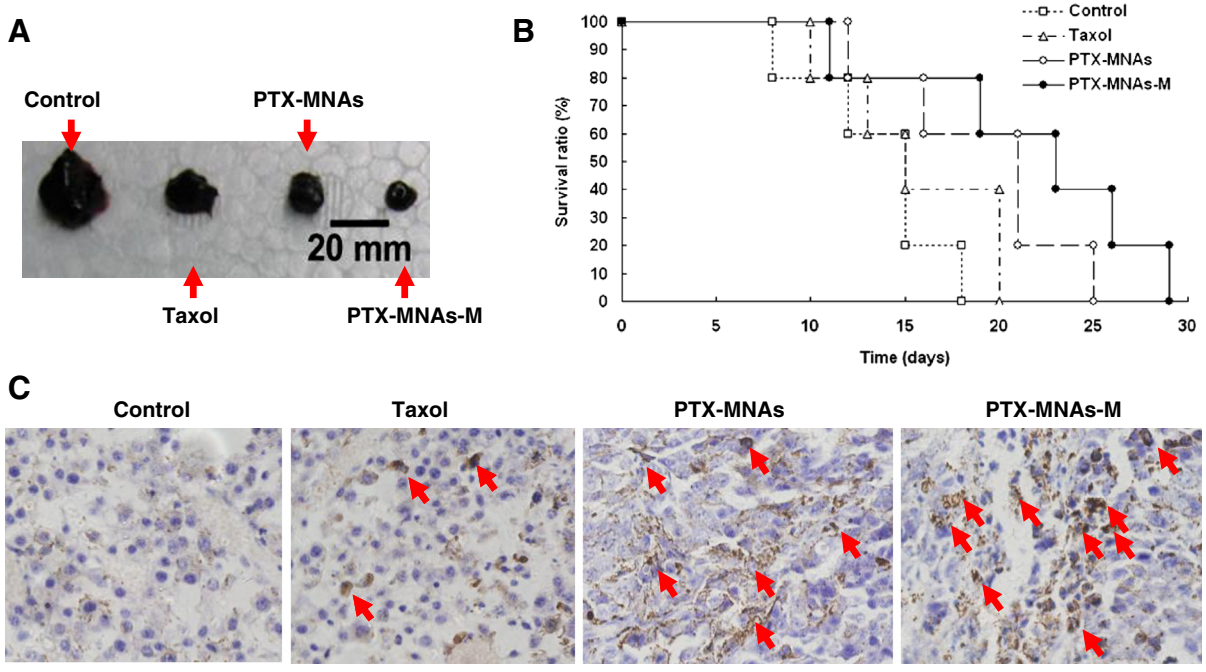

Fig. 4. Antitumor effect of PTX-MNAs in melanoma subcutaneous model. A) Photographs of tumors from each treatment group. B) Kaplan–Meier curves showing survival of mice treated with single dosage of Taxol (free paclitaxel, open triangles), PTX-MNAs in the absence (open circles) and presence of a magnet (filled circles, PTX-MNAs-M). C) Representative micrographs of terminal deoxynucleotidyl transferase-mediated deoxyuridine triphosphate nick-end labeling (TUNEL) assays for apoptotic cell death (magnification 400×). Tumor sections from mice that were given intravenous injection of saline, Taxol (free paclitaxel), and PTX-MNAs in the absence and presence of a magnet (PTX-MNAs-M). Red arrows indicate examples of TUNEL-positive (brown color) cells with apoptotic morphology. (For interpretation of the references to color in this figure legend, the reader is referred to the web version of this article.)

injected intravenously with 10 mg/kg of Taxol, PTX-MNAs, and PTX-MNAs-M, and the PTX levels in biosamples were determined by high performance liquid chromatography (HPLC). The advantages of MNAs carrier for drug circulation in plasma were very obvious (Fig. 6A): PTX in Taxol has a short biological half-life (distribution phase $t_{1/2(\alpha)}$ of 0.47 h, elimination phase $t_{1/2(\beta)}$ of 2.14 h) and rapid elimination rate ($Cl_s = 354.51$ mL/(kg·h)) from the plasma. Loading PTX into MNAs produced a significant change in pharmacokinetic parameters: the PTX-MNAs were more slowly removed from plasma compared with Taxol. The elimination phase ($t_{1/2(\beta)} = 3.63$ h) and mean residence time (MRT = 6.82 h) of PTX-MNAs were 1.7 and 2.2 times longer than those of Taxol, respectively. The area under curve (AUC), elimination rate constant (k_{10}) and Cl_s values also confirmed this trend. An interesting observation was: intravenous administration of PTX-MNAs in the presence of a magnet placed over the surface of mice was also beneficial to increasing amount and prolonging retention time of drug in plasma. There are considerable increases in $t_{1/2(\beta)}$, AUC and MRT parameters and decreases in k_{10} and Cl_s under magnetic field application. Correspondingly, the volume of distribution $V_c = 173.02$ (mL/kg) decreased substantially.

In order to evaluate biodistribution of PTX-MNAs in tumor and other tissues compared with Taxol, some targeting parameters were analyzed in this study [13]. *In vivo* tumor targeting studies displayed variable drug uptake capacity of tumor with different preparations: Re values of PTX-MNAs for plasma and tumor were 1.89 and 2.06, respectively, indicating that the exposure of PTX to plasma and tumor was significantly increased by entrapment of drug into MNAs. Further increase in the Re value caused by application of a magnet over the surface of a tumor was realized: the Re values of PTX-MNAs-M group for plasma and tumor were 2.55 and 3.07, respectively. On the basis of the above results, it can be concluded that encapsulation of PTX into MNAs could improve the drug distribution in plasma and tumor under the same administration dosage as Taxol, and application of an external magnetic field could further increase retention time and accumulation of drug in blood and tumor. The increase was considerable and would induce a better therapeutic effect in tumor diseases.

To further confirm the distribution of vehicles in normal and tumor tissues, Prussian blue staining was performed on tissue sections (Fig. 6B). We found high levels of Prussian blue-positive cells in the liver of the mice that administrated with PTX-MNA. However, liver tissue sections from the group that received PTX-MNAs-M had fewer positive cells. We did not detect iron oxide nanoparticles in the tissue sections of the kidneys from mice injected with either PTX-MNAs or PTX-MNAs-M. TEM provides an even higher resolution and showed the intracellular localization of iron oxide nanoparticles in the cells of tumor tissues (Fig. 6C). Vehicles were internalized within the cell inside cytoplasm and lysosomes. No uptakes of vehicles into mitochondria, endoplasmic reticulum and structures of the Golgi organ or the nucleus were found.

3.5. Safety assay

The changes in body weight and morphological analysis of HE-stained liver and kidneys of healthy mice, which were administered three doses on days 0, 4, and 8 through tail vein, were used as safety

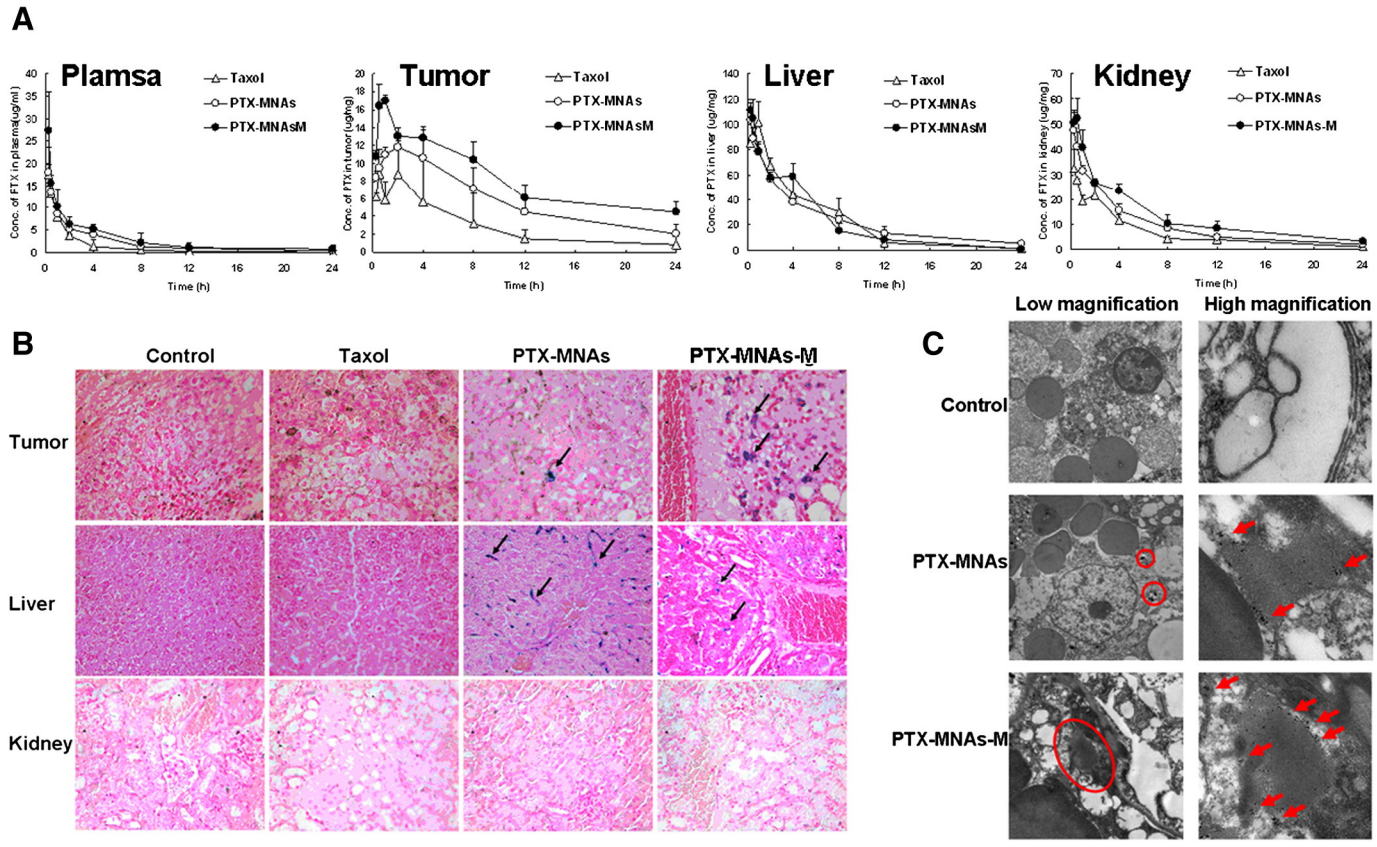

Fig. 6. *In vivo* pharmacokinetics, tissue distribution and accumulation of PTX-MNAs in melanoma subcutaneous model. A) Drug concentration over a period of 24 h is shown for PTX in plasma, tumor, liver and kidneys in C57BL/6 mice receiving an intravenous injection of 10 mg/kg of Taxol (free paclitaxel, open triangles), PTX-MNAs in the absence (open circles) and presence (filled circles) of a magnet ($n = 3$). B) Prussian blue staining images of tumor, liver and kidney obtained from B16F10 cells-implanted C57BL/6 mice treated with saline, Taxol, PTX-MNAs in the absence and presence of a magnet (magnification 400×). Black arrows indicate the presence of iron. C) Low- and high-magnification of TEM images of PTX-MNAs in tumors excised from B16F10 cells-implanted C57BL/6 mice for observing the localization and distribution of iron oxide nanoparticles. Red circles and arrows indicate the presence of iron oxide nanoparticles. (For interpretation of the references to color in this figure legend, the reader is referred to the web version of this article.)

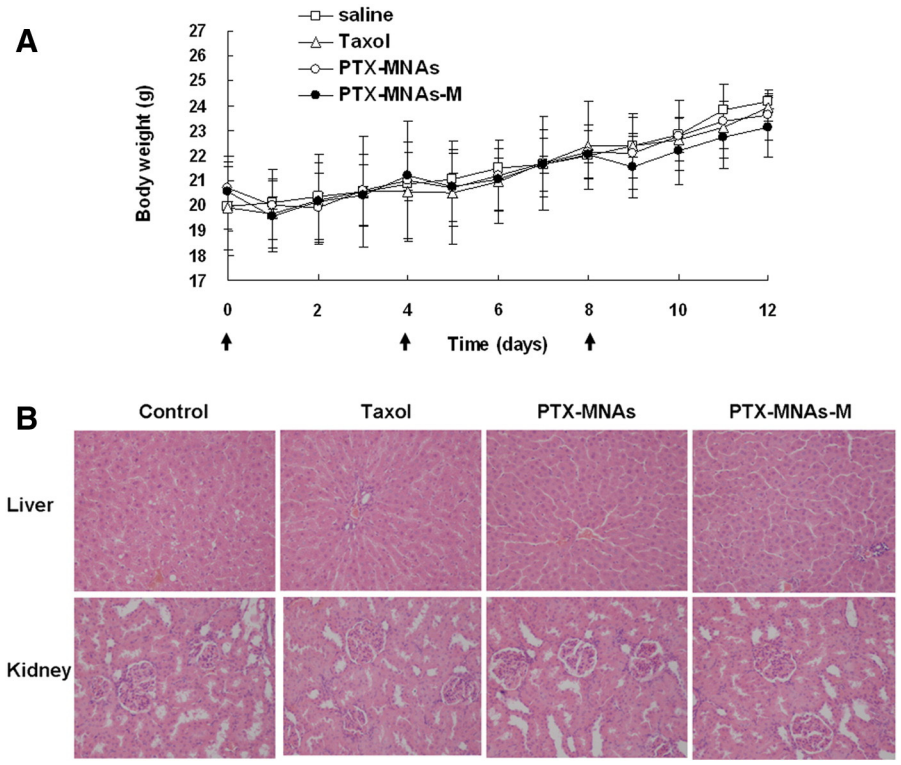

Fig. 7. Systemic toxicity of paclitaxel-loaded magnetic assemblies (PTX-MNAs) in healthy mice. A) Mean body weights in each day of mice administered three doses on days 0, 4, and 8 through tail vein injection of one of the following samples: saline (open squares), Taxol (free paclitaxel, 10 mg PTX/kg, open triangles), and PTX-MNAs (10 mg PTX/kg) in the absence (open circles) and presence (filled circles) of a magnet ($n = 6$). B) Representative histological H&E staining of liver and kidney tissues obtained from healthy mice at day 12 after intravenous injection (magnification 400×).

index. The body weights of mice recovered after cessation of drug treatment and no statistically significant differences in the body weight were observed between the treated mice and saline-injected mice (Fig. 7A). Histological slices in liver and kidneys (Fig. 7B) revealed that PTX-MNAs and PTX-MNAs-M did not cause any inflammatory response, degeneration or necrosis, suggesting the low toxicity of PTX-MNAs in the absence and presence of a magnet. Considered together, PTX-MNAs or PTX-MNAs-M treatment did not induce any apparent toxicity in mice.

4. Conclusions

In summary, we used a simple solvent-exchanging assembly method to load hydrophobic anticancer agents within the inside and outside OA layer of Rubik-like MNAs with rapid and extended release behavior. Assembly of individual nanocube into cluster with high drug loading capability and high magnetism is an effective way to prepare multifunctional theranostic device. These results of cells and animal experiments, as well as the optical imaging data, suggest that significant portions of magnetic nanoassemblies are retained in the tumor after external magnetic field removal and the Rubik-like MNAs in combination with PTX can be effective in reducing tumor size compared with the same dose of free PTX (Taxol). The MR contrast-enhanced imaging can potentially enhance the efficacy of early diagnosis and timely therapeutic intervention. In conclusion, the Rubik-like magnetic nanoassemblies may have the potential to realize "all-in-one" nanotheranostic strategy to detect, diagnose, treat, and monitor tumors and therapeutic response in further pre-clinical and clinical studies.

Acknowledgments

This work was financially supported by National Basic Research Program of China (No. 2011CB933503), National Natural Science Foundation of China (No. 81001412 and 30870689), School of Pharmacy, Fudan University & The Open Project Program of Key Lab of Smart Drug Delivery (Fudan University), Ministry of Education, China and; The Open Project Program of State Key Laboratory of Pharmaceutical Biotechnology (KF-GN-201107), Nanjing University.

References

[1] M. Mahmoudi, M.A. Sahraian, M.A. Shokrgozar, S. Laurent, Superparamagnetic iron oxide nanoparticles: promises for diagnosis and treatment of multiple sclerosis, ACS Chem. Neurosci. 2 (3) (2011) 118–140.
[2] H. He, A. David, B. Chertok, A. Cole, K. Lee, J. Zhang, J.X. Wang, Y.Z. Huang, V.C. Yang, Magnetic nanoparticles for tumor imaging and therapy: a so-called theranostic system, Pharm. Res. (Jan 24 2013), http://dx.doi.org/10.1007/s11095-013-0982-y(Epub ahead of print).
[3] K.H.J. Buschow, Handbook of Magnetic Materials, 16, Elsevier Science, Amsterdam, 2006.
[4] I. Brigger, C. Dubernet, P. Couvreur, Nanoparticles in cancer therapy and diagnosis, Adv. Drug Deliv. Rev. 54 (5) (2002) 631–651.
[5] H. Ai, C. Flask, B. Weinberg, X. Shuai, M.D. Pagel, D. Farrell, J. Duerk, J. Gao, Magnetite-loaded polymeric micelles as ultrasensitive magnetic-resonance probes, Adv. Mater. 17 (16) (2005) 1949–1952.
[6] J. Kim, J.E. Lee, S.H. Lee, J.H. Yu, J.H. Lee, T.G. Park, T. Hyeon, Designed fabrication of a multifunctional polymer nanomedical platform for simultaneous cancer-targeted imaging and magnetically guided drug delivery, Adv. Mater. 20 (3) (2008) 478–483.
[7] D.C. Niu, Y.S. Li, Z. Ma, H. Diao, J.L. Gu, H.R. Chen, W.R. Zhao, M.L. Ruan, Y.L. Zhang, J.L. Shi, Preparation of uniform, water-soluble, and multifunctional nanocomposites with tunable sizes, Adv. Funct. Mater. 20 (5) (2010) 773–780.
[8] H. Tan, J.M. Xue, B. Shuter, X. Li, J. Wang, Synthesis of PEOlated Fe_3O_4@SiO_2 nanoparticles via bioinspired silification for magnetic resonance imaging, Adv. Funct. Mater. 20 (5) (2010) 722–731.
[9] A. Ditsch, P.E. Laibinis, D.I.C. Wang, T.A. Hatton, Controlled clustering and enhanced stability of polymer-coated magnetic nanoparticles, Langmuir 21 (13) (2005) 6006–6018.
[10] J.E. Lee, N. Lee, H. Kim, J. Kim, S.H. Choi, J.H. Kim, T. Kim, I.C. Song, S.P. Park, W.K. Moon, T. Hyeon, Uniform mesoporous dye-doped silica nanoparticles decorated with multiple magnetite nanocrystals for simultaneous enhanced magnetic resonance imaging, fluorescence imaging, and drug delivery, J. Am. Chem. Soc. 132 (2) (2010) 552–557.

[11] F. Danhier, O. Feron, V. Préat, To exploit the tumor microenvironment: passive and active tumor targeting of nanocarriers for anti-cancer drug delivery, J. Control. Release 148 (2) (2010) 135–146.
[12] N.R. Jana, Y.F. Chen, X.G. Peng, Size- and shape-controlled magnetic (Cr, Mn, Fe, Co, Ni) oxide nanocrystals via a simple and general approach, Chem. Mater. 16 (20) (2004) 3931–3935.
[13] Y.J. Chen, J. Tao, F. Xiong, J.B. Zhu, N. Gu, Y.H. Zhang, Y. Ding, L. Ge, Synthesis, self-assembly, and characterization of PEG-coated iron oxide nanoparticles as potential MRI contrast agent, Drug Dev. Ind. Pharm. 36 (10) (2010) 1235–1244.
[14] M.J. Song, Y. Zhang, S.L. Hu, L.N. Song, J.L. Dong, Z.P. Chen, N. Gu, Influence of morphology and surface exchange reaction on magnetic properties of monodisperse magnetite nanoparticles, Colloids Surf. A. 5 (39) (2012) 1–8.